



**IMPLEMENTING MULTI-SCALE AGRICULTURAL INDICATORS EXPLOITING SENTINELS**

**VEGETATION FIELD DATA AND PRODUCTION OF  
GROUND-BASED MAPS:**

**“OTTAWA SITE, CANADA”  
MAY TO AUGUST 2014**

**ISSUE I1.00**

EC Proposal Reference N° FP7-311766

Actual submission date : June 2015

Start date of project: 01.11.2012

Duration : 40 months

**Name of lead partner for this deliverable: EOLAB**



Book Captain: Consuelo Latorre (EOLAB)

Contributing Authors: Fernando Camacho (EOLAB)

E. Pattey (CFIA)

<b>Project co-funded by the European Commission within the Seventh Framework Program (2007-2013)</b>		
<b>Dissemination Level</b>		
PU	Public	<b>X</b>
PP	Restricted to other programme participants (including the Commission Services)	
RE	Restricted to a group specified by the consortium (including the Commission Services)	
CO	Confidential, only for members of the consortium (including the Commission Services)	

## DOCUMENT RELEASE SHEET

<b>Book Captain:</b>	C. Latorre	Date: 15.06.2015	Sign. 
<b>Approval:</b>	R. Lacaze	Date: 10.12.2015	Sign. 
<b>Endorsement:</b>	I. Marin-Moreno	Date:	Sign.
<b>Distribution:</b>	Public		

## CHANGE RECORD

Issue/Revision	Date	Page(s)	Description of Change	Release
	15.06.2015	All	First Issue	I1.00

## TABLE OF CONTENTS

<b>1. Background of the Document</b>	<b>12</b>
1.1. Executive Summary	12
1.2. Portfolio	12
1.3. Scope and Objectives	13
1.4. Content of the Document	13
<b>2. Introduction</b>	<b>14</b>
5 <sup>th</sup> to 11 <sup>th</sup> of June 2014	15
23 <sup>th</sup> to 27 <sup>th</sup> of June 2014	15
2 <sup>nd</sup> to 10 <sup>th</sup> of July 2014	15
<b>3. Study area</b>	<b>16</b>
3.1. Location	16
3.2. Description of The Test Site	17
<b>4. Ground measurements</b>	<b>18</b>
4.1. Material and Methods	18
4.1.1 Standard Digital Photography (SDP)	18
4.1.2 LI190SB / LI-191R	20
4.1.3 LI-3100C Area meter	21
4.2. Spatial Sampling Scheme	22
4.3. Measurement protocol	23
4.4. ground data	24
4.3.1 Data processing	24
4.3.2 Content of the Ground Dataset	25
8 <sup>th</sup> June 2014	29
25 <sup>th</sup> June 2014	29
<b>5. Evaluation of the sampling</b>	<b>31</b>
5.1. Evaluation Based On NDVI Values	31
5.2. Evaluation Based On Convex Hull: Product Quality Flag	32
<b>6. Production of ground-based maps</b>	<b>35</b>
6.1. Imagery	35
6.2. The Transfer Function	35
6.2.1 The regression method	35

6.2.2	Band combination .....	36
6.2.3	The selected Transfer Function .....	37
<b>6.3.</b>	<b>The High Resolution Ground Based Maps .....</b>	<b>40</b>
6.3.1	Mean Values .....	42
<b>7.</b>	<b>Conclusions .....</b>	<b>44</b>
<b>8.</b>	<b>Acknowledgements.....</b>	<b>45</b>
<b>9.</b>	<b>References .....</b>	<b>46</b>

## LIST OF FIGURES

<i>Figure 1: Ottawa site, Canada. Left: Location of the site. Middle: Footprint of Landsat-8 tiles. Right: 5x5 km<sup>2</sup> footprint of the study area over GoogleEarth image. ....</i>	16
<i>Figure 2: Example of a Corn field in Ottawa (Canada) from JECAM (2014). ....</i>	17
<i>Figure 3: False color composition (RGB: SWIR-NIR-Red) Landsat-8 TOC Reflectance images over the 5x5 km<sup>2</sup> study area (Ottawa, Canada) for three dates (8<sup>th</sup> June, 25<sup>th</sup> June, 29<sup>th</sup> July, 2014). ....</i>	17
<i>Figure 4: LI190SB Quantum Sensor .....</i>	20
<i>Figure 5: LI-191R .....</i>	21
<i>Figure 6: LI-3100C. ....</i>	21
<i>Figure 7: Distribution of the sampling units (ESUs) over the study 5x5 km<sup>2</sup> area. Example Landsat-8 TOC false color composition SWIR-NIR-Red, over GoogleEarth for the first campaign 8<sup>th</sup> June, 2014. Ottawa, Canada. ....</i>	22
<i>Figure 8: LAIeff measurements from SDP. The period of selected campaigns is shown in colored vertical rectangles. ....</i>	26
<i>Figure 9: Green LAI/PAI measurements (destructive) and PAIeff (indirect method) over several fields. The period of selected campaigns is shown in colored vertical rectangles. ....</i>	26
<i>Figure 10: Continuous FAPAR measurements over Wheat fields (ESU #5 and ESU #6). The period of selected campaigns is shown in colored vertical rectangles. ....</i>	27
<i>Figure 11: FCOVER measurements over several fields. The period of selected campaigns is shown in colored vertical rectangles. ....</i>	27
<i>Figure 12: LAIeff measurements acquired in Ottawa site (Canada), during the field campaigns 2014. Four field campaigns: First (8<sup>th</sup> June), Second (25<sup>th</sup> June), Third (6<sup>th</sup> July) and Fourth (29<sup>th</sup> July); ESU1-6: Wheat fields; ESU7: Canola; ESU8-11: Soybean; ESU12-15: Corn. ....</i>	28
<i>Figure 13: FCOVER measurements acquired in Ottawa site (Canada), during the field campaigns 2014. Four field campaigns: First (8<sup>th</sup> June), Second (25<sup>th</sup> June), Third (6<sup>th</sup> July) and Fourth (29<sup>th</sup> July); ESU1-6: Wheat fields; ESU7: Canola; ESU8-11: Soybean; ESU12-15: Corn. ....</i>	28
<i>Figure 14: Distribution of the measured LAIeff over the ESUs. Ottawa site, multi-temporal field campaigns, 2014. ....</i>	29
<i>Figure 15: Distribution of the measured FCOVER over the ESUs. Ottawa site, multi-temporal field campaigns, 2014. ....</i>	29
<i>Figure 16: Comparison of NDVI distribution between ESUs and over the whole site (5 highest and 5 lowest cumulative frequencies). Multi-temporal field campaign, Ottawa site (Canada), 2014. ....</i>	32
<i>Figure 17: Convex Hull over 5x5 km<sup>2</sup> area. Clear and dark blue correspond to the pixels belonging to the 'strict' and 'large' convex hulls. Red corresponds to the pixels for which the transfer function behaves as extrapolator. Ottawa - Canada, 2014. ....</i>	33
<i>Figure 18: Landsat-8 TOC Reflectance. Test of multiple regressions (TF) applied on different band combinations for LAIeff. Band combinations are given in abscissa (1=Green 2=Red, 3=NIR and 4=SWIR). ....</i>	36
<i>Figure 19: Landsat-8 TOC Reflectance. Test of multiple regressions (TF) applied on different band combinations for FCover. Band combinations are given in abscissa (1=Green 2=Red, 3=NIR and 4=SWIR). ....</i>	37
<i>Figure 20: LAIeff, results for regression on NDVI over Landsat-8 image. Full dots: Weight&gt;0.7. Empty dots: 0&lt;Weight&lt;0.7. Crosses: Weight=0. ....</i>	39
<i>Figure 21: FCover results for regression on NDVI over Landsat-8 image. Full dots: Weight&gt;0.7. Empty dots: 0&lt;Weight&lt;0.7. Crosses: Weight=0. ....</i>	39

*Figure 22: Landsat-8 LAIeff ground-based maps (5x5 km<sup>2</sup>) over the Ottawa site (Canada). The central date of each ground campaign is considered as representative of the ground map: 8<sup>th</sup> June (top left), 25<sup>th</sup> June (top right), 6<sup>th</sup> July (bottom left) and 29<sup>th</sup> July (bottom right), 2014. .... 40*

*Figure 23: Landsat-8 FCOVER ground-based maps (5x5 km<sup>2</sup>) over the Ottawa site (Canada). The central date of each ground campaign is considered as representative of the ground map: 8<sup>th</sup> June (top left), 25<sup>th</sup> June (top right), 6<sup>th</sup> July (bottom left) and 29<sup>th</sup> July (bottom right), 2014. .... 41*

*Figure 24: LAIeff versus FCOVER scatter plots for the Landsat-8 ground-based maps. Ottawa site (Canada). 8<sup>th</sup> June (top left), 25<sup>th</sup> June (top right), 6<sup>th</sup> July (bottom left) and 29<sup>th</sup> July (bottom right) ..... 42*



## LIST OF TABLES

---

<i>Table 1: Ground Campaign dates and Landsat-8 imagery available. "Mean date" is the day of the period where the majority of the ESUs are concentrated. ....</i>	<i>15</i>
<i>Table 2: Coordinates and altitude of the test site (centre).....</i>	<i>16</i>
<i>Table 3: Cardinality of ESUs measurements, globally and for each land cover class in Ottawa site (Canada).....</i>	<i>23</i>
<i>Table 4: Total of measurements collected over the Ottawa site (Canada). Cardinality of measurements by crop type and by variable.....</i>	<i>24</i>
<i>Table 5: The Header used to describe ESUs with the ground measurements. ....</i>	<i>25</i>
<i>Table 6: Landsat-8 image. Percentages over the test site of Ottawa (Canada). Convex hull values: 0=extrapolation of TF, 1=strict convex hull and 2=large convex hull. ....</i>	<i>33</i>
<i>Table 7: Acquisition properties of Landsat-8 data used for producing empirical high resolution maps. ....</i>	<i>35</i>
<i>Table 8: Transfer function applied to the whole site over Landsat-8 image for LAI<sub>eff</sub> and FCOVER. RW (weighted RMSE), RC (cross-validation RMSE). ....</i>	<i>38</i>
<i>Table 9. Mean values and standard deviation (STD) of the HR biophysical Landsat-8 maps for the selected 3 x 3 km<sup>2</sup> area at Ottawa site (Canada). ....</i>	<i>42</i>
<i>Table 10: Content of the dataset.....</i>	<i>43</i>

## LIST OF ACRONYMS

---

<b>AAFC</b>	Agriculture and Agri-Food Canada
<b>CEOS</b>	Committee on Earth Observation Satellite
<b>CEOS LPV</b>	Land Product Validation Subgroup
<b>CFIA</b>	Canadian Food Inspection Agency
<b>DG AGRI</b>	Directorate General for Agriculture and Rural Development
<b>DG RELEX</b>	Directorate General for External Relations (European Commission)
<b>SDP</b>	Standard Digital Photos
<b>ECV</b>	Essential Climate Variables
<b>EUROSTATS</b>	Directorate General of the European Commission
<b>ESU</b>	Elementary Sample Unit
<b>FAPAR</b>	Fraction of Absorbed Photo-synthetically Active Radiation
<b>FAO</b>	Food and Agriculture Organization
<b>FCOVER</b>	Fraction of Vegetation Cover
<b>GCOS</b>	Global Climate Observing System
<b>GEO-GLAM</b>	Global Agricultural Geo- Monitoring Initiative
<b>GIO-GL</b>	GMES Initial Operations - Global Land (GMES)
<b>GCOS</b>	Global Climate Observing System
<b>GMES</b>	Global Monitoring for Environment and Security
<b>GPS</b>	Global Positioning System
<b>IDL</b>	Interactive Data Language
<b>IMAGINES</b>	Implementing Multi-scale Agricultural Indicators Exploiting Sentinels
<b>JECAM</b>	Joint Experiment for Crop Assessment and Monitoring
<b>MSG</b>	Meteosat Second Generation satellite
<b>LAI</b>	Leaf Area Index
<b>LDAS</b>	Land Data Assimilation System
<b>LIDF</b>	Leaf Inclination Distribution Function
<b>LUT</b>	Look-up-table techniques
<b>OLIVE</b>	On Line Validation Exercise
<b>PAI</b>	Plant Area Index
<b>PROBA-V</b>	Project for On-Board Autonomy satellite, the V standing for vegetation.
<b>PSF</b>	Point Spread Function
<b>RMSE</b>	Root Mean Square Error
<b>SPOT /VGT</b>	<i>Satellite Pour l'Observation de la Terre</i> / VEGETATION
<b>SLT</b>	Solar Local Time
<b>SSOT</b>	<i>Sistema Satelital para la Observación de la Tierra</i>
<b>STD</b>	STandard Deviation

<b>TOC</b>	Top of Canopy Reflectance
<b>USGS</b>	U.S. Geological Survey Science organization
<b>UNFCCC</b>	United Nations Framework Convention on Climate Change
<b>UTM</b>	Universal Transverse Mercator coordinates system
<b>VALERI</b>	Validation of Land European Remote sensing Instruments
<b>WGCV</b>	Working Group on Calibration and Validation (CEOS)

# 1. BACKGROUND OF THE DOCUMENT

## 1.1. EXECUTIVE SUMMARY

The Copernicus Land Service has been built in the framework of the FP7 geoland2 project, which has set up pre-operational infrastructures. ImagineS intends to ensure the continuity of the innovation and development activities of geoland2 to support the operations of the global land component of the GMES Initial Operation (GIO) phase. In particular, the use of the future Sentinel data in an operational context is prepared. Moreover, IMAGINES favors the emergence of new downstream activities dedicated to the monitoring of crop and fodder production.

The main objectives of ImagineS are to (i) improve the retrieval of basic biophysical variables, mainly LAI, FAPAR and the surface albedo, identified as Terrestrial Essential Climate Variables, by merging the information coming from different sensors (PROBA-V and Landsat-8) in view to prepare the use of Sentinel missions data; (ii) develop qualified software able to process multi-sensor data at the global scale on a fully automatic basis; (iii) complement and contribute to the existing or future agricultural services by providing new data streams relying upon an original method to assess the above-ground biomass, based on the assimilation of satellite products in a Land Data Assimilation System (LDAS) in order to monitor the crop/fodder biomass production together with the carbon and water fluxes; (iv) demonstrate the added value of this contribution for a community of users acting at global, European, national, and regional scales.

Further, ImagineS serves the growing needs of international (e.g. FAO and NGOs), European (e.g. DG AGRI, EUROSTATS, DG RELEX), and national users (e.g. national services in agro-meteorology, ministries, group of producers, traders) on accurate and reliable information for the implementation of the EU Common Agricultural Policy, of the food security policy, for early warning systems, and trading issues. ImagineS will also contribute to the Global Agricultural Geo-Monitoring Initiative (GEO-GLAM) by its original agriculture service which can monitor crop and fodder production together with the carbon and water fluxes and can provide drought indicators, and through links with JECAM (Joint Experiment for Crop Assessment and Monitoring).

## 1.2. PORTFOLIO

The ImagineS portfolio contains global and regional biophysical variables derived from multi-sensor satellite data, at different spatial resolutions, together with agricultural indicators, including the above-ground biomass, the carbon and water fluxes, and drought indices resulting from the assimilation of the biophysical variables in the Land Data Assimilation System (LDAS).

The production in Near Real Time of the 333m resolution products, at a frequency of 10 days, using PROBA-V data is carried out in the Copernicus Global Land Service.

The demonstration of high resolution (30m) products derived from Landsat-8 is done over demonstration sites of cropland and grassland in contrasting climatic and environmental conditions.

### 1.3. SCOPE AND OBJECTIVES

The main objective of this document is to describe the field campaign and ground data collected at Ottawa site, Canada, and the up-scaling of the ground data to produce ground-based high resolution maps of the following biophysical variables:

- Leaf Area Index (LAI), defined as half of the total developed area of leaves per unit ground surface area ( $m^2/m^2$ ). We focused on two different LAI quantities (for green elements):
  - The effective LAI (LAI<sub>eff</sub>) derived from the description of the gap fraction as a function of the view zenith angle.
  - The actual LAI, derived from destructive measurements.
- Fraction of green Vegetation Cover (FCover), defined as the proportion of soil covered by vegetation, derived from the gap fraction between 0 and 10° of view zenith angle.
- Fraction of Absorbed Photosynthetically Active Radiation (FAPAR), which is the fraction of the photosynthetically active radiation (PAR) absorbed by a vegetation canopy. PAR is the solar radiation reaching the canopy in the 0.4–0.7  $\mu m$  wavelength region.

Due to the reduced number of measurements for green LAI and for FAPAR, only LAI<sub>eff</sub> and FCover have been up-scaled (see Section 6).

### 1.4. CONTENT OF THE DOCUMENT

This document is structured as follows:

- Chapter 2 provides an introduction to the field experiment.
- Chapter 3 provides the location and description of the site.
- Chapter 4 describes the ground measurements, including material and methods, sampling and data processing.
- Chapter 5 provides an evaluation of the sampling.
- Chapter 6 describes the production of high resolution ground-based maps, and the selected “mean” values for validation.

## 2. INTRODUCTION

Validation of remote sensing products is mandatory to guaranty that the satellite products meets the user's requirements. Protocols for validation of global LAeff products are already developed in the context of Land Product Validation (LPV) group of the Committee on Earth Observation Satellite (CEOS) for the validation of satellite-derived land products (Fernandes et al., 2014), and recently applied to Copernicus global land products based on SPOT/VGT observation (Camacho et al., 2013). This generic approach is made of 2 major components:

- The indirect validation: including inter-comparison between products as well as evaluation of their temporal and spatial consistency
- The direct validation: comparing satellite products to ground measurements of the corresponding biophysical variables. In the case of low and medium resolution sensors, the main difficulty relies on scaling local ground measurements to the extent corresponding to pixels size. However, the direct validation is limited by the small number of sites, for that reason a main objective of ImagineS is the collection of ground truth data in demonstration sites.

The content of this document is compliant with existing validation guidelines (for direct validation) as proposed by the CEOS LPV group (Morissette et al., 2006); the VALERI project (<http://w3.avignon.inra.fr/valeri/>) and ESA campaigns (Baret and Fernandes, 2012). It therefore follows the general strategy based on a bottom up approach: it starts from the scale of the individual measurements that are aggregated over an elementary sampling unit (ESU) corresponding to a support area consistent with that of the high resolution imagery used for the up-scaling of ground data. Several ESUs are sampled over the site. Radiometric values over a decametric image are also extracted over the ESUs. This will be later used to develop empirical transfer functions for up-scaling the ESU ground measurements (e.g. Martínez et al., 2009). Finally, the high resolution ground based map will be compared with the medium resolution satellite product at the spatial support of the product.

One of the demonstration sites of ImagineS is located at the Canadian Food Inspection Agency (CFIA) experimental farm in Ottawa, Ontario, Canada. A multi-temporal campaign to characterize the biophysical parameters of different crop types over the test site from May to August of 2014 was carried out by AgriFood, in the context of its regular ground monitoring activities.

EOLAB has grouped the closest observations performed within an interval lower than 10 days in four periods and considering that the number of available ESUs was at least eight in order to perform the up-scaling with high resolution Landsat-8 images. Table 1 describes the period of the field data acquisition for each campaign, and the valid Landsat-8 imagery dates used for the definition of the Transfer Function. Three cloud-free Landsat-8 images were available through the USGS Global Visualization Viewer service (<http://glovis.usgs.gov/> )

**Multi-temporal Field Campaigns:** 14<sup>th</sup> May to 24<sup>th</sup> August, 2014.

**Table 1: Ground Campaign dates and Landsat-8 imagery available. “Mean date” is the day of the period where the majority of the ESUs are concentrated.**

Campaigns	Mean date	Period	Imagery
<b>First campaign</b>	8 <sup>th</sup> June	5 <sup>th</sup> to 11 <sup>th</sup> of June 2014	Landsat-8 TOC (02.06.2014)
<b>Second campaign</b>	25 <sup>th</sup> June	23 <sup>th</sup> to 27 <sup>th</sup> of June 2014	Landsat-8 TOC (27.06.2014)
<b>Third campaign</b>	6 <sup>th</sup> July	2 <sup>nd</sup> to 10 <sup>th</sup> of July 2014	Landsat-8 TOC (27.06.2014)
<b>Fourth campaign</b>	29 <sup>th</sup> July	25 <sup>th</sup> July to 1 <sup>st</sup> August 2014	Landsat-8 TOC (29.07.2014)

**Team involved in field collection:**

E. Pattey, G. Jégo (CFIA)

A. Vanderzaag, J. Liu, B.Qian, W. Smith, X. Geng (CFIA)

**Contact:**

CFIA: Elizabeth Pattey – Elizabeth.Pattey@agr.gc.ca

EOLAB: Fernando Camacho - fernando.camacho@eolab.es

### 3. STUDY AREA

#### 3.1. LOCATION

“Ottawa” site is located closed to the capital city of Canada, in the southern Ontario province (Figure 1, Left). Ottawa is located at the confluence of three rivers: the Ottawa River, the Gatineau River and the Rideau River. The study site sits on a flat area. The centroid is at latitude 45° 18' 19.48” N, longitude 75° 46' 1.66” W. (Table 2).

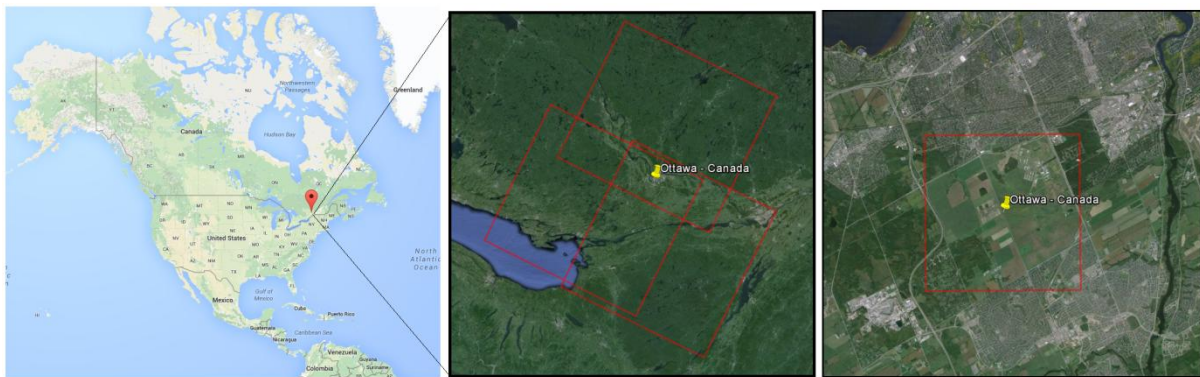


**Figure 1: Ottawa site, Canada. Left: Location of the site. Middle: Footprint of Landsat-8 tiles. Right: 5x5 km<sup>2</sup> footprint of the study area over GoogleEarth image.**

**Table 2: Coordinates and altitude of the test site (centre).**

Site Center	
Geographic Lat/lon, WGS-84 (degrees) UTM zone 18N.	Latitude = 45° 18' 19.48” N Longitude = 75° 46' 1.66” W
Altitude	90 m



### 3.2. DESCRIPTION OF THE TEST SITE

The CFIA experimental farm in Ottawa includes three major field crops cultivated in Eastern Canada: corn, soybean and wheat. Field data were collected during the growing season of 2014. The climate is humid continental, with an average of 732 mm of rain and 236mm of snow per year, and temperature averages from 13.4°C to 20.9°C from May to August. The crop calendar extends from 1<sup>st</sup> May to end of October. Figure 2 shows an image of a corn field (JECAM report, 2014).



Figure 2: Example of a Corn field in Ottawa (Canada) from JECAM (2014).

Figure 3 shows the false color composition of the three Landsat-8 TOC Reflectance images selected for up-scaling. The evolution of the vegetation over the different fields can be observed.

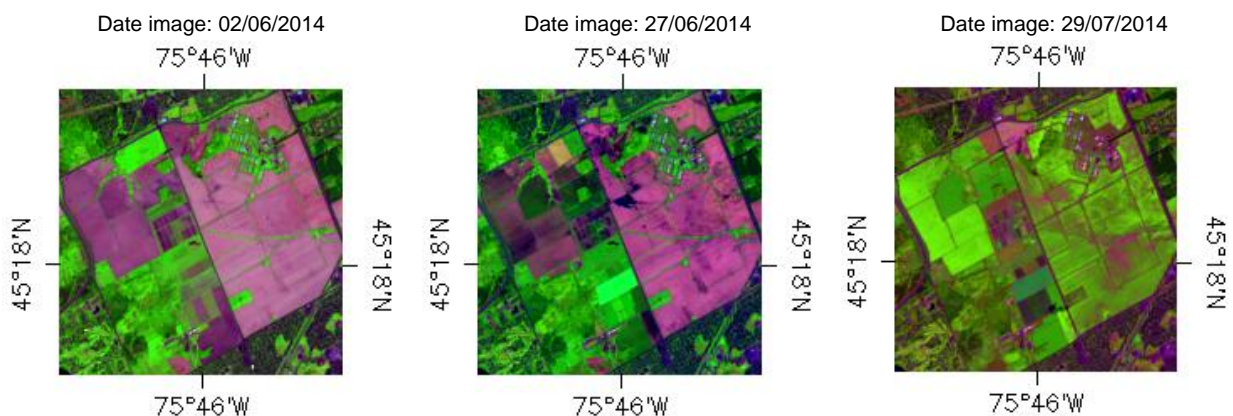


Figure 3: False color composition (RGB: SWIR-NIR-Red) Landsat-8 TOC Reflectance images over the 5x5 km<sup>2</sup> study area (Ottawa, Canada) for three dates (8<sup>th</sup> June, 25<sup>th</sup> June, 29<sup>th</sup> July, 2014).

## 4. GROUND MEASUREMENTS

The ground measurement database reported here was collected at the Canadian Food Inspection Agency (CFIA) experimental farm in Ottawa, Ontario. EOLAB has grouped the dataset for up-scaling several field campaigns. (see associated **2014\_VGM\_Ottawa.xls** file).

### 4.1. MATERIAL AND METHODS

#### 4.1.1 Standard Digital Photography (SDP)

Standard Digital Photography (SDP) and Digital Hemispherical Photos (DHP) allow the calculation of LAI, and FCOVER of field crops by quantifying gap fraction either at nadir or at a 57.5° view angle. The Green Area Index (GAI) derived for corn, soybean and wheat crops was strongly linearly correlated with the destructive GAI for both the nadir and the 57.5° photographic methods (Liu et al., 2013).

Thanks to recent technological developments, digital cameras with high spatial and radiometric resolutions are becoming increasingly affordable, promoting the use of digital photographic methods to quantify canopy structural variables. Equipment such as a plant canopy analyzers or a digital camera with a fisheye lens (DHP) acquire the information over a range of angles. In contrast, a digital camera with a rectilinear lens can only obtain unidirectional information, however, the practical advances of this approach are the simplicity of the measurement protocol, the processing of digital photographs and the condition required to operate are less restriction on radiation conditions. A major advantage of digital photography over other non-destructive methods is that a digital camera can be used under both direct and diffuse light conditions with no need for a reference measurement (Liu et al., 2013). Standard digital photography taken at a restricted field of view provides better spatial resolution than the corresponding hemispherical photos and thus would improve the differentiation of green vegetation tissues from soil or non-green vegetation tissues (Baret et al., 2010).

Vertical photography is conventionally used to measure canopy fractional coverage, although foliage projection is most sensitive to leaf angle distribution in the vertical viewing direction. LAI could be derived from gap fraction measured from this direction using the assumption of a spherical leaf angle distribution, with performance comparable to that obtained using LAI-2000 in corn, soybean and wheat crops (Liu and Pattey, 2012).

Digital colour photos were taken from above the canopy looking downward vertically. Each pixel of a photo consists of three digital numbers which are light intensity quantized in the red, green and blue bands. The photos were processed using a histogram-based threshold method to separate green leaf tissues from background soils and residue. Crop vertical gap fraction and LAI were then derived following Liu and Pattey (2010).

The first step was to estimate canopy structural descriptors from a standard digital photograph to derive the greenness of the images:

$$\text{Greenness} = 2 \cdot G - B - R \quad \text{Eq.(1)}$$

This transformation exploits the high contrast between the reflected light intensity of green leaves and other scene elements, including background soil, residue and stems. The derived greenness is also resistant to leaf mirror reflection as long as a portion of the radiation interacts with chlorophyll. A sequential procedure was developed to extract canopy vertical gap fraction from the calculated greenness image using a threshold approach based on histogram analysis. First, the greenness and its histogram are calculated for a digital photograph. The histogram is then smoothed with a low pass filter to remove high frequency noise. The next step is to determine a threshold from the histogram. In the last step, vertical green gap fraction is directly obtained from the cumulative histogram (Liu and Pattey, 2010).

The rectilinear digital photos were processed using the **GreenCropTracker** software, which was implemented with a histogram thresholding algorithm to differentiate gaps from plant tissues. The tool was developed using IDL (Interactive Data Language) and is able to process both nadir and 57.5° photographs taken in upward or downward-looking directions ([www.flintbox.com/public/project/5470](http://www.flintbox.com/public/project/5470)). It derives biophysical variables from gap fraction measurements as follows:

**Effective LAI (LAI<sub>eff</sub>):** Assuming the foliage is azimuthally uniform and spatially randomly distributed, the relationship between canopy gap fraction and LAI<sub>eff</sub> is given by the Poisson distribution (Nilson, 1971). Eq. (2) and Eq. (3)

$$P_0(\theta_v, \varphi_v) = e^{-N \cdot (\theta_v, \varphi_v)} = e^{-G \cdot (\theta_v, \varphi_v) \cdot \frac{LAI_{eff}}{\cos(\theta_v)}} \quad \text{Eq. (2)}$$

$$LAI_{eff} = \frac{-\cos(\theta) \cdot \ln(P_0(\theta))}{G(\theta)} = -\frac{\ln(P_0(\theta))}{k(\theta)} \quad \text{Eq. (3)}$$

Where  $P_0(\theta)$  is the gap fraction in view or solar zenith angle  $\theta$ ,  $G(\theta)$  is the foliage projection coefficient for the plane perpendicular to direction  $\theta$ , and  $k(\theta)$  is canopy extinction coefficient. A Clumping index was estimated using the logarithmic averaging method of Lang and Xiang (1986) to derive the total GAI.

When a photograph is taken looking vertically downward (i.e.,  $\theta=0^\circ$ ), vertical gap fraction can be directly measured by calculating the proportion of background pixels (including non-green leaf materials) to the total pixels within the frame of the photo. A spherical LIDF (Leaf Inclination Distribution Function) is considered a good first-order approximation for crop canopies, in which case  $G$  is equal to 0.5 at any direction (Goudriaan, 1988). LAI is thus estimated from the vertical gap fraction assuming spherical LIDF as follows:

$$LAI_{eff} = -2 \cdot \ln(P_0(0)) \quad \text{Eq. (4)}$$

Plant canopy analyzer such as LAI-2000 has been used to compare with the results derived from SDP. It measures simultaneously gap fraction with five rings, corresponding to different zenith angles, using a hemispherical lens, and canopy LAI is calculated from the

measurements through a weighted sum approach (Li-Cor, 1992) using the following formula as implemented in LAI-2000:

$$LAI_{eff} = -2 \cdot \sum_{i=1}^5 \ln(P_0(\theta_i)) \cdot \cos(\theta_i) \cdot \sin(\theta_i) \cdot \Delta\theta_i \quad \text{Eq. (5)}$$

**FCOVER** is retrieved from gap fraction as 1- gap fraction ( $\theta=0$ ).

#### 4.1.2 LI190SB / LI-191R

LI190SB and LI-191R Quantum Sensor (LI-COR, 2013) were used for the continuous measurement of incoming PAR, canopy-reflected PAR, soil incoming PAR, soil-reflected PAR. The LI190SB measures solar radiation with a silicon photovoltaic detector mounted in a cosine-corrected head (Figure 4). A shunt resistor in the sensor's cable converts the signal from microamps to millivolts, allowing the LI190SB to be measured directly by a Campbell Scientific datalogger.

LI190SB accurately measures Photosynthetic Photon Flux Density (PPFD), which is the number of photons in the 400 to 700 nm waveband incident per unit time on a unit surface. Because PPFD describes photosynthetic activity, the LI190SB is ideal for growth chambers and greenhouses. (<http://www.campbellsci.com/li190sb-l>)



Figure 4: LI190SB Quantum Sensor

A non-uniform light field under a plant canopy is difficult to characterize with a single sensor or multiple sensors arranged in a line because the light field can vary considerably from point to point and over a line.

To solve this problem, the entire LI-191R diffuser is sensitive to light over its 1-meter length (Figure 5). Since the diffuser is one continuous piece, the LI-191R essentially integrates an infinite number of points over its surface into a single value that represents light from the entire 1-meter length. ([http://www.licor.com/env/products/light/quantum\\_line.html](http://www.licor.com/env/products/light/quantum_line.html))



**Figure 5: LI-191R**

Sensors that use multiple photodiodes potentially induce large uncertainty in measurements because each photodiode can drift independently of the others. The diffuser and single photodiode in the LI-191R provide stable, integrated measurements that are superior to averages provided by many linear sensors.

Optical filters block radiation with wavelengths beyond 700 nm, which is critical for under-canopy measurements, where the ratio of infrared to visible light may be high.

The FAPAR was then accurately estimated with the quantum sensors by the closure of the energy as follows:

$$FAPAR = PAR_{incoming} - PAR_{reflected} - PAR_{soil} + PAR_{reflected\_soil} \quad \text{Eq. (6)}$$

#### 4.1.3 LI-3100C Area meter

The LI-3100C (Licor, 2013) Area Meter is a planimeter designed for efficient and exacting area measurement of both large and small leaves (Figure 6). A wide variety of leaves can be measured, ranging from larger samples such as corn to smaller samples such as wheat, rice or alfalfa. Small leaves or leaf discs are measured with the same precision as larger leaves. The LI-3100C can also handle conifer needles, perforated leaves and leaves with irregular margins.



**Figure 6: LI-3100C.**

Samples are placed between the guides on the lower transparent belt and allowed to pass through the LI-3100C. As the sample travels under the fluorescent light source, the projected image is reflected by a system of three mirrors to a scanning camera. An adjustable press

roller flattens curled leaves and feeds them properly between the transparent belts. This provides for accurate measurement of small grasses, legumes, aquatic plants and similar types of leaves. As samples pass under the light source, the accumulating area in mm<sup>2</sup> is shown on the LED display or on a computer screen when using the Windows® software. ([http://www.licor.com/env/products/leaf\\_area/LI-3100C/](http://www.licor.com/env/products/leaf_area/LI-3100C/))

**LAI:** The actual LAI was measured with the planimeter LI-3100C. Eq. (7) shows the relationship between LAI and LA<sub>eff</sub> where  $\lambda_0$  is the clumping index.

$$LAI_{eff} = \lambda_0 \cdot LAI \quad \text{Eq. (7)}$$

## 4.2. SPATIAL SAMPLING SCHEME

A pseudo-regular sampling was used within each ESU of approximately 20x20 m<sup>2</sup>, around 12 measurements per ESU from nadir and from 57.5° for SDP. A maximum of 19 ESUs were characterized per "campaign" (Table 3). The centre of the ESU was geo-located.

The sampling scheme for the first field campaign collection (all ESUS) is shown Figure 7. The ground measurements are spread across fields of corn, soybean, wheat and canola.

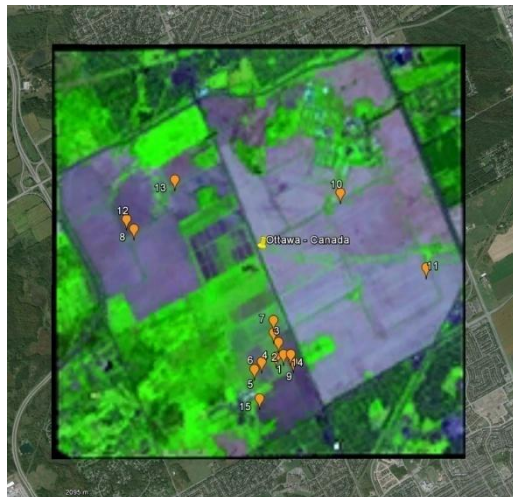


**Figure 7: Distribution of the sampling units (ESUS) over the study 5x5 km<sup>2</sup> area. Example Landsat-8 TOC false composition SWIR-NIR-Red, over GoogleEarth for the first campaign 8<sup>th</sup> June, 2014. Ottawa, Canada.**

Table 3 summarizes the number sampling units (ESUs) characterized per each crop type during the field campaigns.



**Table 3: Cardinality of ESUs measurements, globally and for each land cover class in Ottawa site (Canada).**

Land Use	Number of ESU's			
	First campaign	Second campaign	Third campaign	Fourth campaign
	5 <sup>th</sup> to 11 <sup>th</sup> of June	23 <sup>th</sup> to 27 <sup>th</sup> of June	2 <sup>nd</sup> to 10 <sup>th</sup> of July	25 <sup>th</sup> July to 1 <sup>st</sup> August
Wheat	6	4	5	6
Soybean	4	2	4	1
Corn	5	2	4	2
Canola	4	-	-	1
<b>TOTAL</b>	<b>19</b>	<b>8</b>	<b>13</b>	<b>10</b>

### 4.3. MEASUREMENT PROTOCOL

This section describes the measurement protocol for each variable. All the variables refers to green elements.

- **LAI<sub>eff</sub>**

SDP taken with camera (Nikon Coolpix P500) facing down (up for corn > 1 m tall) along two transects separated by 10 m with 4 m between photos. 3 to 9 times per site; SDP processed with GreenCropTracker program.

LAI<sub>eff</sub> (57°) taken with standard digital camera (Nikon Coolpix S4). Photos taken with camera angled at 57.5° along two transects separated by 10 m with 4 m between photos. 1 to 7 times per site; SDP processed with GreenCropTracker program.

- **LAI and PAI**

Take above ground biomass from an ESU (wheat - one third of 5 square areas of 0.25 m<sup>2</sup> each, canola - 3 of 5 square areas of 0.25 m<sup>2</sup> each, corn - 5 of 15 plants, soybean - 5 of 15 plants); separate into stem, green leaf, dead leaf, reproductive; measure area of parts using LI3100 (excluding corn stems). 2 to 5 times per site.

- **FAPAR**

Continuous measure of incoming PAR, canopy-reflected PAR, soil incoming PAR, soil-reflected PAR measured with LI190SB Quantum Sensor and Li191 Line Quantum Sensor Ratios of daily totals of APAR and PAR; (See equation 6).

$$APAR = PAR - PAR_{reflected} - PAR_{soil} + PAR_{reflected_{soil}} \quad \text{Eq. (8)}$$

- **FCOVER**

Photos taken with camera facing down (up for corn > 1 m tall) along two transects separated by 10 m with 4 m between photos. 3 to 9 times per site; estimated processing SDP with GreenCropTracker program.

## 4.4. GROUND DATA

### 4.3.1 Data processing

Standard Digital Photography has been used in addition to the conventional equipment (LI3100, LI190SB and LI191) for acquiring measurements over the field crops before they reach full canopy closure. The software **GreenCropTracker** was used to process the SDP images.

**Table 4: Total of measurements collected over the Ottawa site (Canada). Cardinality of measurements by crop type and by variable.**

Classification per type of cropland						
Number of Measurements						
METHOD	Wheat	Canola	Soybean	Corn	TOTAL	
Destructive Sampling	21	4	6	3	264	
SDP	27	5	19	21		
Li190SB/Li192	158	-	-	-		
Number of total samples						
METHOD	Wheat	Canola	Soybean	Corn	TOTAL	
Destructive Sampling	105	12	30	15	5406	
SDP	397	56	248	286		
Li190SB/Li192	4257	-	-	-		
Classification per Variable						
Number of Measurements						
METHOD	FAPAR	PAI <sub>eff</sub>	LAI <sub>57eff</sub>	FCOVER	Green PAI	Green LAI
Destructive Sampling					34	34
SDP		72	53	69		
Li190SB/Li192	158					
<b>TOTAL</b>	<b>158</b>	<b>72</b>	<b>53</b>	<b>69</b>	<b>34</b>	<b>34</b>



Table 4 shows a summary of the measurements collected during the multi-temporal field campaigns. A total of 264 measures (5406 samples) were performed with the different methods of acquisition, of which 420 values were extracted for six biophysical variables (FAPAR, PAI<sub>eff</sub>, LAI<sub>57eff</sub>, FCOVER, green PAI and green LAI).

### 4.3.2 Content of the Ground Dataset

Each ESU is described according to a standard format. The header of the database is shown in Table 5.

**Table 5: The Header used to describe ESUs with the ground measurements.**

Column	Var.Name	Comment
1	Plot #	Number of the field plot in the site
2	Plot Label	Label of the plot in the site
3	ESU #	Number of the Elementary Sampling Unit (ESU)
4	ESU Label	Label of the ESU in the campaign
5	Northing Coord.	Geographical coordinate: Latitude (°), WGS-84
6	Easting Coord.	Geographical coordinate: Longitude (°), WGS-84
7	Extent (m) of ESU (diameter)	Size of the ESU <sup>(1)</sup>
8	Land Cover	Detailed land cover
9	Start Date (dd/mm/yyyy)	Starting date of measurements
10	End Date (dd/mm/yyyy)	Ending date of measurements
11	Products*	Method
12		Nb. Replications
13		Products*
14		Uncertainty
		Instrument
		Number of Replications
		Methodology
		Standard deviation

\*LAI<sub>eff</sub>, LAI, FAPAR and FCOVER

Figure 8 to Figure 11 show the temporal variation over 2 ESUs for Soybean (ESU 8 and ESU 9), Corn (ESU 12 and ESU 14) and Wheat (ESU 5 and ESU 6), during the field experiment.

For LAI<sub>eff</sub> (Figure 8), soybean fields show a rapid increase from end of June to mid July with maximum LAI<sub>eff</sub> values (actually PAI<sub>eff</sub>) of 6. Similar phenology was observed for Corn field, starting in early June and reaching the maximum LAI<sub>eff</sub> values (around 4) at the end of July. Wheat fields started at the end of May or early June, and reaches the maximum values (LAI<sub>eff</sub> = 5) around the second 'campaign' by end of June. The colored vertical bars represent the period of the four field campaigns. Ground data (squares, diamonds) within green bars have been used for up-scaling.

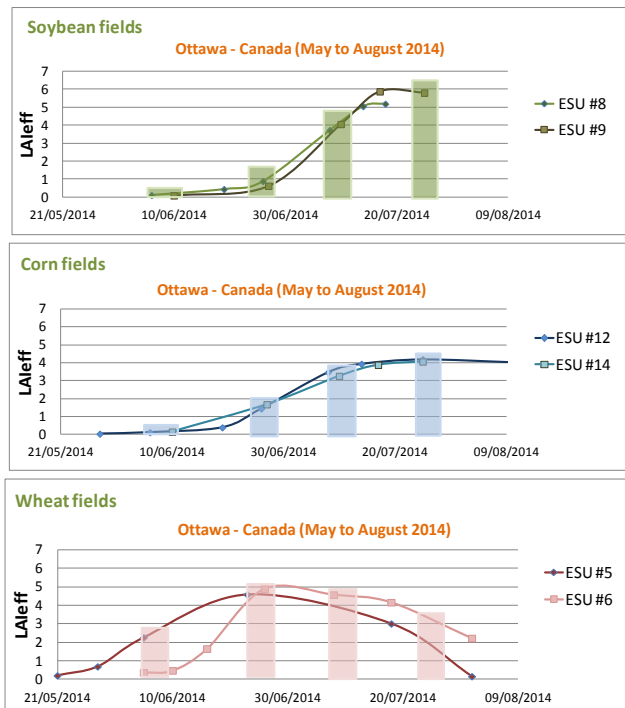


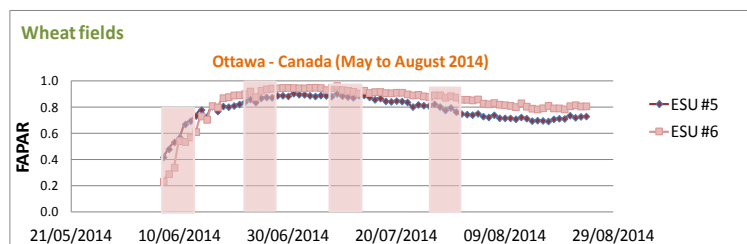
Figure 8: LAIeff measurements from SDP. The period of selected campaigns is shown in colored vertical rectangles.



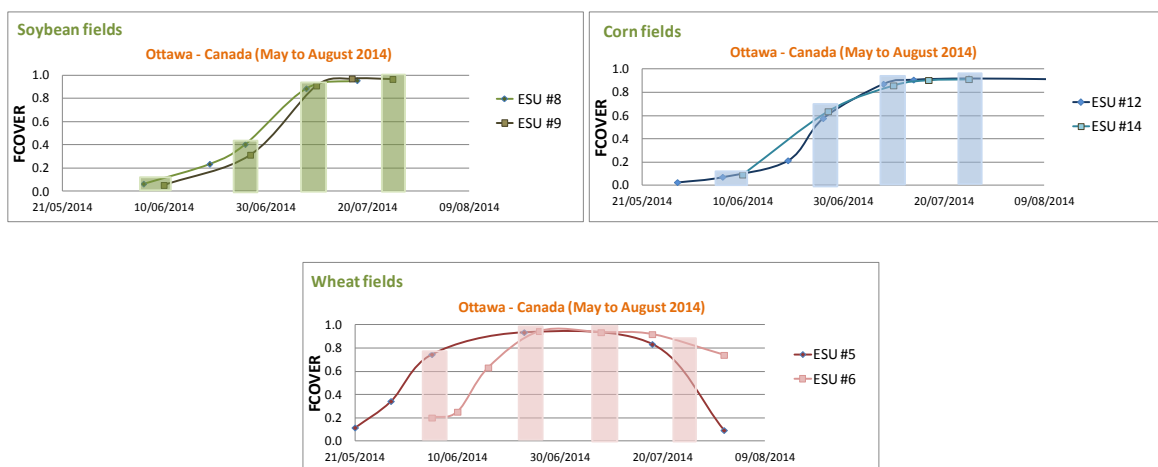
Figure 9: Green LAI/PAI measurements (destructive) and PAIeff (indirect method) over several fields. The period of selected campaigns is shown in colored vertical rectangles.

Figure 9 shows the green LAI, green PAI evolution for several ESU of each crop type. As expected the differences between LAI and PAI increases during the senescent period, where the maturation of the spikes becomes more important, which is clearly observed for wheat fields. However, in the early stages of growing the green PAI and the green LAI are very similar. This confirms the idea that accuracy assessment of satellite vegetation products (related to green elements) in croplands should be performed during the first stages of the plant development. Note also that the LAI<sub>eff</sub> estimated with indirect methods (Standard Photo), which corresponds to a PAI<sub>eff</sub>, will be also affected by the increase of stems and other plant elements which are typically more important during the maturation and senescence. Note that for the soybean field an important difference (positive) of the PAI<sub>eff</sub> is observed as compared to the destructive green PAI measurement for the maximum development. This is partly due to presence of non-green elements and errors in the processing of the SDP.

FAPAR was measured continuously in two ESUS of wheat fields. Figure 10 shows the phenology during three months. During the interval of the first campaign (10 days) the wheat fields showed quick growing of about 0.4 FAPAR units.



**Figure 10: Continuous FAPAR measurements over Wheat fields (ESU #5 and ESU #6). The period of selected campaigns is shown in colored vertical rectangles.**



**Figure 11: FCOVER measurements over several fields. The period of selected campaigns is shown in colored vertical rectangles.**

Figure 11 shows FCover measurements. Two ESUs per field have been chosen to evaluate the evolution during all the period.

A more exhaustive analysis of the LA<sub>eff</sub> and FCover variables have been evaluated per ESU as both variables have been up-scaled using high resolution maps.

Figure 12 shows the LA<sub>eff</sub> measurements obtained during the field experiment grouped per 'campaigns'. LA<sub>eff</sub> shows maximum values ranging from 2.1 (First campaign) to 5.8 (Fourth campaign). Maximum values are reported for Wheat (ESUs 1 to 6) in the second campaign (23-27 June) and for Soybean (ESUs 8-11) in the fourth campaign.

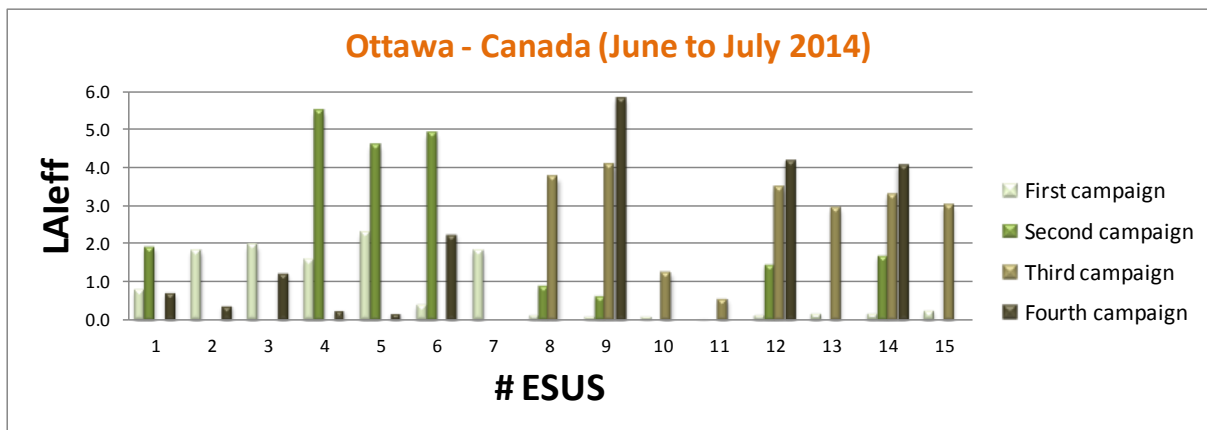


**Figure 12: LA<sub>eff</sub> measurements acquired in Ottawa site (Canada), during the field campaigns 2014. Four field campaigns: First (8<sup>th</sup> June), Second (25<sup>th</sup> June), Third (6<sup>th</sup> July) and Fourth (29<sup>th</sup> July); ESU1-6: Wheat fields; ESU7: Canola; ESU8-11: Soybean; ESU12-15: Corn.**

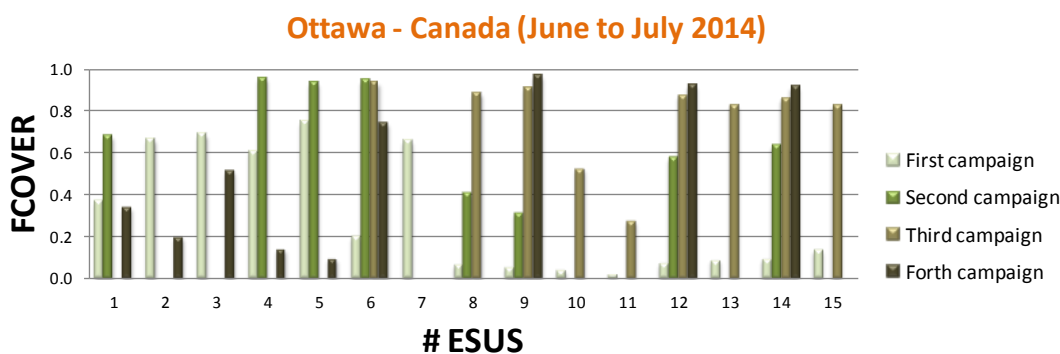


**Figure 13: FCOVER measurements acquired in Ottawa site (Canada), during the field campaigns 2014. Four field campaigns: First (8<sup>th</sup> June), Second (25<sup>th</sup> June), Third (6<sup>th</sup> July) and Fourth (29<sup>th</sup> July); ESU1-6: Wheat fields; ESU7: Canola; ESU8-11: Soybean; ESU12-15: Corn.**

For the FCover (Figure 13), we can observe a large variability from very low values to very high, in almost all the ESUs. Maximum values reached more than 0.9 in the second campaign for Wheat (ESUs1-6) and in the fourth campaign for Soybean (ESUs 8-11) and Corn fields (ESUs 12-15).

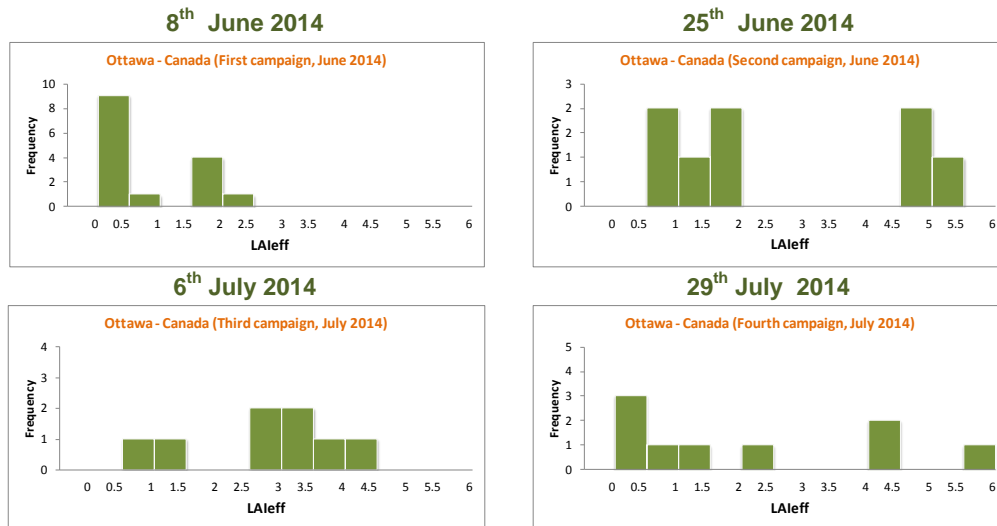


**Figure 14: Distribution of the measured LAleff over the ESUs. Ottawa site, multi-temporal field campaigns, 2014.**

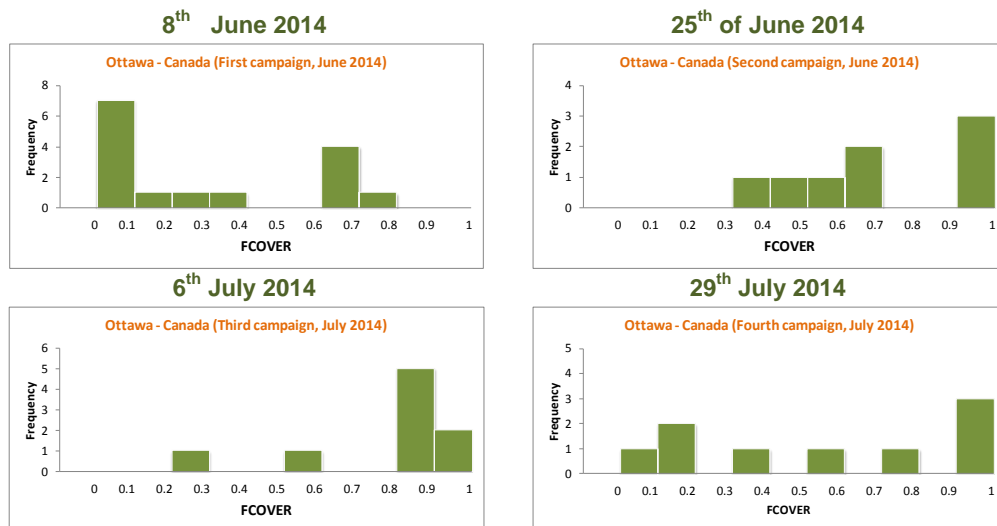


**Figure 15: Distribution of the measured FCOVER over the ESUs. Ottawa site, multi-temporal field campaigns, 2014.**

Figure 14 and Figure 15 show the distribution of the measured LAleff and FCover variables. The largest frequencies are observed for low values in the first campaign, while for

the other campaigns there are typically 1-3 observations distributed from low to high values. Note that in the second and third campaign there is no observation for very low values (below 0.5 for LAI, and 0.2-0.3 for FCOVER).

## 5. EVALUATION OF THE SAMPLING

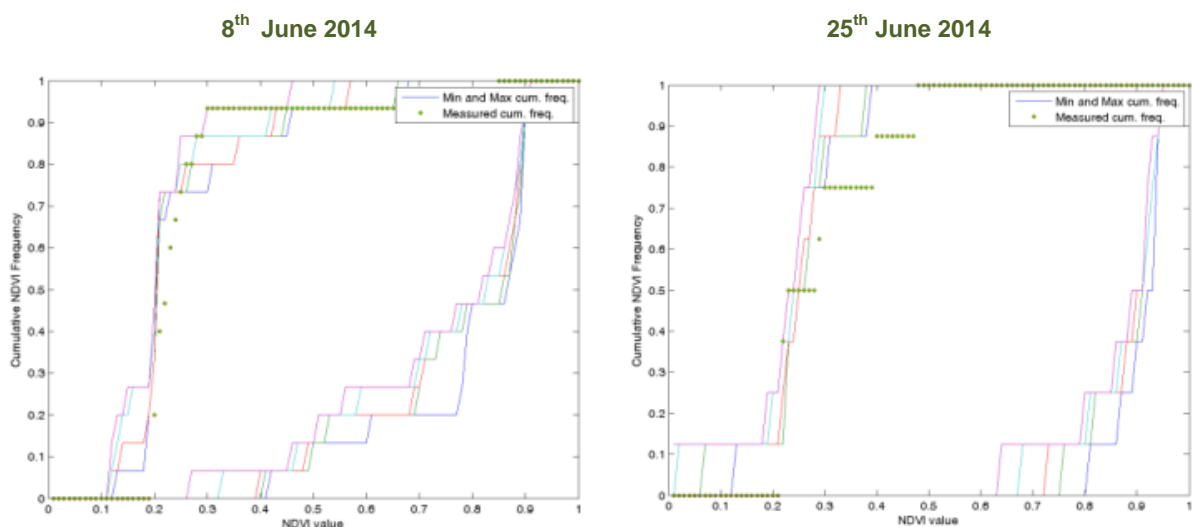
### 5.1. EVALUATION BASED ON NDVI VALUES

The sampling strategy is evaluated using the Landsat-8 image by comparing the NDVI distribution over the site with the NDVI distribution over the ESUs (Figure 16). As the number of pixels is drastically different for the ESU and the whole site (WS), it is not statistically consistent to directly compare the two NDVI histograms. Therefore, the proposed technique consists in comparing the NDVI cumulative frequency of the two distributions by a Monte-Carlo procedure which aims at comparing the actual frequency to randomly shifted sampling patterns. It consists in:

1. computing the cumulative frequency of the  $N$  pixel NDVI that correspond to the exact ESU locations; then, applying a unique random translation to the sampling design (modulo the size of the image)
2. computing the cumulative frequency of NDVI on the randomly shifted sampling design
3. repeating steps 1 and 2, 199 times with 199 different random translation vectors.

This provides a total population of  $N = 199 + 1$ (actual) cumulative frequency on which a statistical test at acceptance probability  $1 - \alpha = 95\%$  is applied: for a given NDVI level, if the actual ESU density function is between two limits defined by the  $N\alpha / 2 = 5$  highest and lowest values of the 200 cumulative frequencies, the hypothesis assuming that WS and ESU NDVI distributions are equivalent is accepted, otherwise it is rejected.

Figure 16 shows that the NDVI distributions over the ESUs, are close to the lowest cumulative frequencies for the four campaigns. That means that the sampling is biased towards the lower NDVI values in the  $5 \times 5 \text{ km}^2$  area.



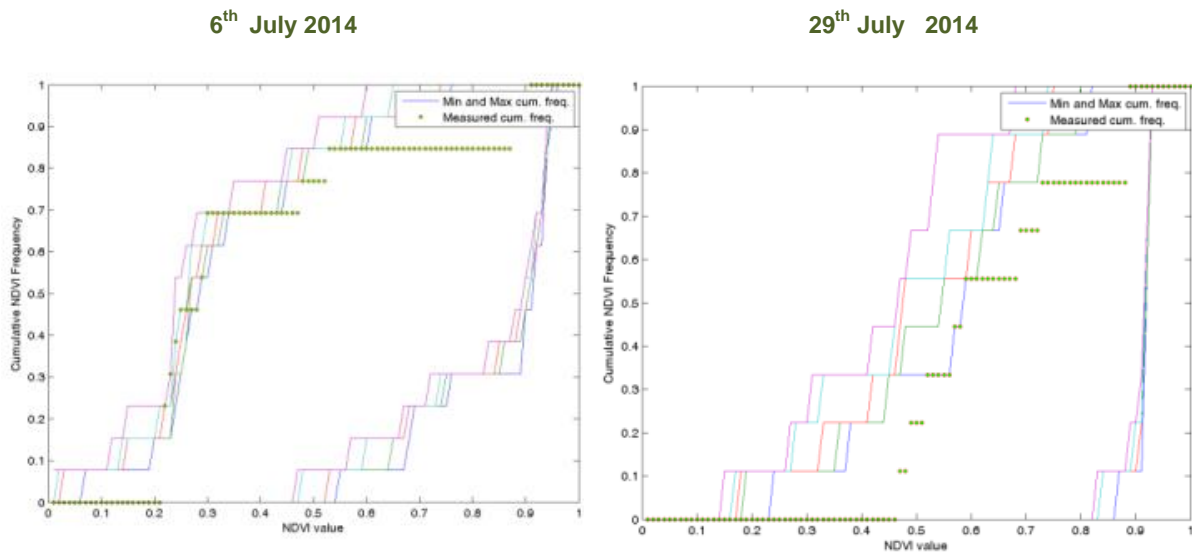


**Figure 16: Comparison of NDVI distribution between ESUs and over the whole site (5 highest and 5 lowest cumulative frequencies). Multi-temporal field campaign, Ottawa site (Canada), 2014.**

## 5.2. EVALUATION BASED ON CONVEX HULL: PRODUCT QUALITY FLAG.

The interpolation capabilities of the empirical transfer function used for up-scaling the ground data using decametric images is dependent of the sampling (Martinez et al., 2009). A test based on the convex hulls was also carried out to characterize the representativeness of ESUs and the reliability of the empirical transfer function using the different combinations of the selected bands of the Landsat-8 TOC image. A flag image is computed over the TOC reflectance, for the band combination used for generating the empirical biophysical maps: NIR and Red bands (i.e. NDVI) were selected for up-scaling ground data with Landsat-8 imagery (see Section 6.2 for details). The result on convex-hulls can be interpreted as:

- pixels inside the 'strict convex-hull': a convex-hull is computed using all the Landsat-8 TOC reflectance corresponding to the ESUs belonging to the class. These pixels are well represented by the ground sampling and therefore, when applying a transfer function the degree of confidence in the results will be quite high, since the transfer function will be used as an interpolator;
- pixels inside the 'large convex-hull': a convex-hull is computed using all the reflectance combinations ( $\pm 5\%$  in relative value) corresponding to the ESUs. For these pixels, the degree of confidence in the obtained results will be quite good, since the transfer function is used as an extrapolator (but not far from interpolator);
- pixels outside the two convex-hulls: this means that for these pixels, the transfer function will behave as an extrapolator which makes the results less reliable. However,



having a priori information on the site may help to evaluate the extrapolation capacities of the transfer function.

**Table 6: Landsat-8 image. Percentages over the test site of Ottawa (Canada). Convex hull values: 0=extrapolation of TF, 1=strict convex hull and 2=large convex hull.**

Campaign	Quality Flags (%)											
Landsat8	5x5 km <sup>2</sup>											
DATE	8 <sup>th</sup> June			25 <sup>th</sup> June			6 <sup>th</sup> July			29 <sup>th</sup> July		
Convex hull	0	1	2	0	1	2	0	1	2	0	1	2
values	81%	17%	2%	77%	12%	11%	48%	25%	27%	71%	9%	20%

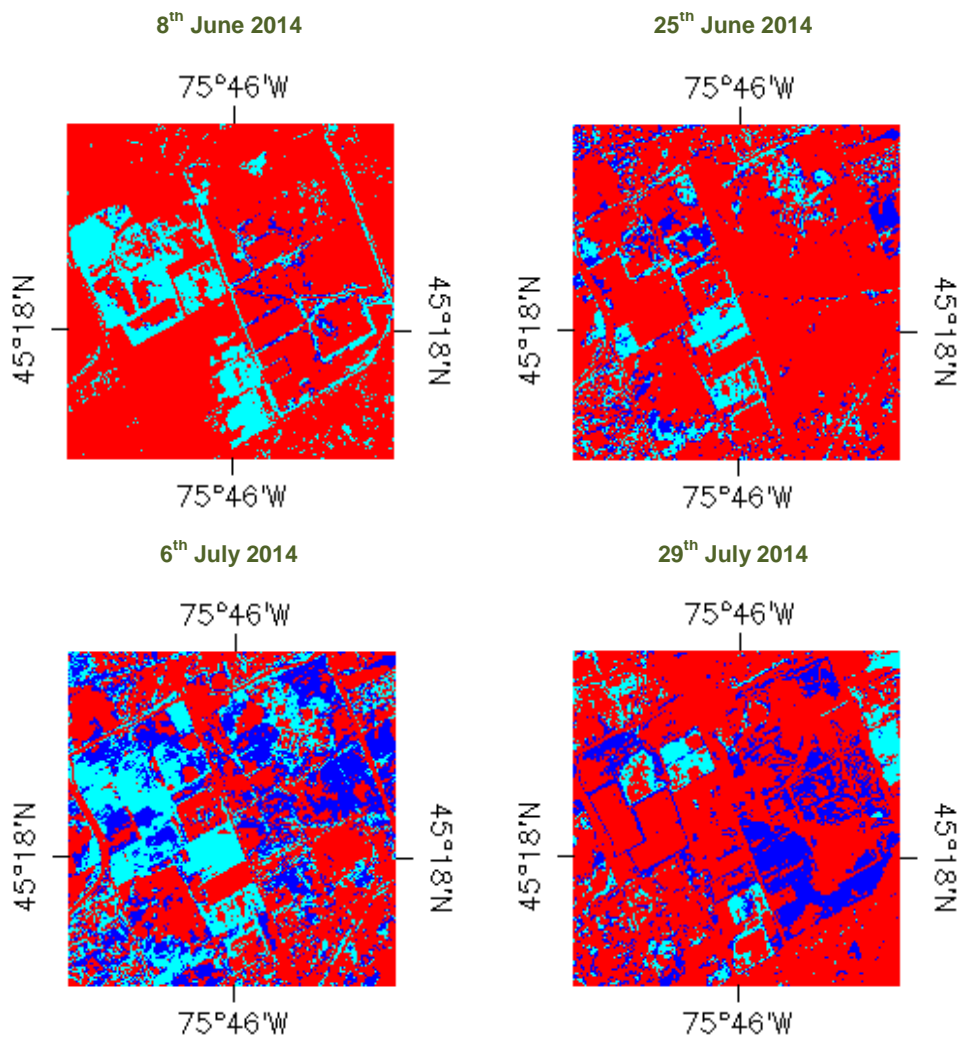


**Figure 17: Convex Hull over 5x5 km<sup>2</sup> area. Clear and dark blue correspond to the pixels belonging to the 'strict' and 'large' convex hulls. Red corresponds to the pixels for which the transfer function behaves as extrapolator. Ottawa - Canada, 2014.**

Figure 17 shows the results of the Convex-Hull test (i.e. Quality Flag images) for the Ottawa site over the 5x5 km<sup>2</sup> study area. The strict and large convex-hulls are high around the ESUs (blue color), although the percentage for the four field campaigns over the total area are 19%, 23%, 52% and 29% for the selected combination band over Landsat-8 image (Table 6). Note that the pixels flagged as of lower quality (i.e. where the transfer function behaves as extrapolator i.e. Quality Flag=0) correspond in most cases to bare soil areas that were not sampled during the field experiment.

## 6. PRODUCTION OF GROUND-BASED MAPS

### 6.1. IMAGERY

The Landsat-8 images were acquired the 2<sup>nd</sup> June, 27<sup>th</sup> June and 29<sup>th</sup> July, 2014 (see Table 7 for acquisition properties). We selected 4 spectral bands from 500 nm to 1750 nm with a nadir ground sampling distance of 30 m. For the transfer function analysis, the input satellite data used is Top of Canopy (TOC) reflectance. The original projection is UTM 18 North, WGS-84.

**Table 7: Acquisition properties of Landsat-8 data used for producing empirical high resolution maps.**

Landsat-8 TOC METADATA				
Platform / Instrument	Landsat-8 / OLI_TIRS			
Sensor	OPTICAL 30 m			
Selected spectral range	B3(green) : 0.53-0.59 $\mu\text{m}$ B4(red) : 0.64-0.67 $\mu\text{m}$ B5(NIR) : 0.85-0.88 $\mu\text{m}$ B6(SWIR1) : 1.58-1.65 $\mu\text{m}$			
Field campaigns 2014	<b>First campaign</b>	<b>Second &amp; Third campaign</b>		<b>Fourth campaign</b>
	8 <sup>th</sup> June	25 <sup>th</sup> June	6 <sup>th</sup> of July	29 <sup>th</sup> July
Acquisition date	02/06/2014 15:50:39	27/06/2014 15:44:35		29/07/2014 15:44:48
Path	16	15		15
Row	29			
doy	153	178		210
Illumination azimuth angle	139.76°	136.37°		139.97°
Illumination solar angle	26.84°	26.50°		30.88°

### 6.2. THE TRANSFER FUNCTION

#### 6.2.1 The regression method

If the number of ESUs is enough, multiple robust regressions 'REG' between ESUs reflectance and the considered biophysical variable can be applied (Martínez et al., 2009): we used the 'robustfit' function from the Matlab statistics toolbox. It uses an iteratively re-weighted least squares algorithm, with the weights at each iteration are computed by applying the bi-square function to the residuals from the previous iteration. This algorithm provides lower weight to ESUs that do not fit well.

The results are less sensitive to outliers in the data as compared with ordinary least squares regression. At the end of the processing, two errors are computed: weighted RMSE (RW) (using the weights attributed to each ESU) and cross-validation RMSE (RC) (leave-one-out method).

As the method has limited extrapolation capacities, a flag image for each transfer function (Figure 17), are included in the ground based maps in order to inform the users on the reliability of the estimates.

### 6.2.2 Band combination

Figure 18 and Figure 19 show the errors (RW, RC) obtained for the several band combinations using TOC reflectance for LA<sub>eff</sub> and FCOVER respectively. In this particular case, where we have very few points for constraining the empirical function, we have selected the NDVI as input for the transfer function (exponential relationship with LAI, and linear relationship with FCover, see section 6.2.3). NDVI does not show in some cases the lower errors (eg. third campaign for LA<sub>eff</sub> and first campaign for FCOVER) but assures good consistency of the LA<sub>eff</sub> and FCOVER maps over the whole area, as can be observed in Figure 22 and Figure 23. This was not the case for other combinations, where large inconsistencies between LA<sub>eff</sub> and FCOVER were found over the site.

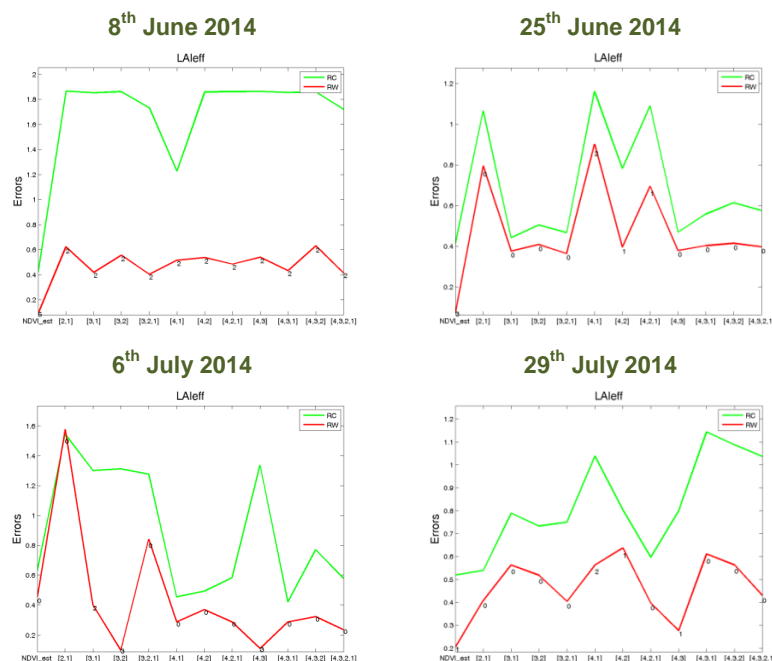


**Figure 18: Landsat-8 TOC Reflectance. Test of multiple regressions (TF) applied on different band combinations for LA<sub>eff</sub>. Band combinations are given in abscissa (1=Green 2=Red, 3=NIR and 4=SWIR).**

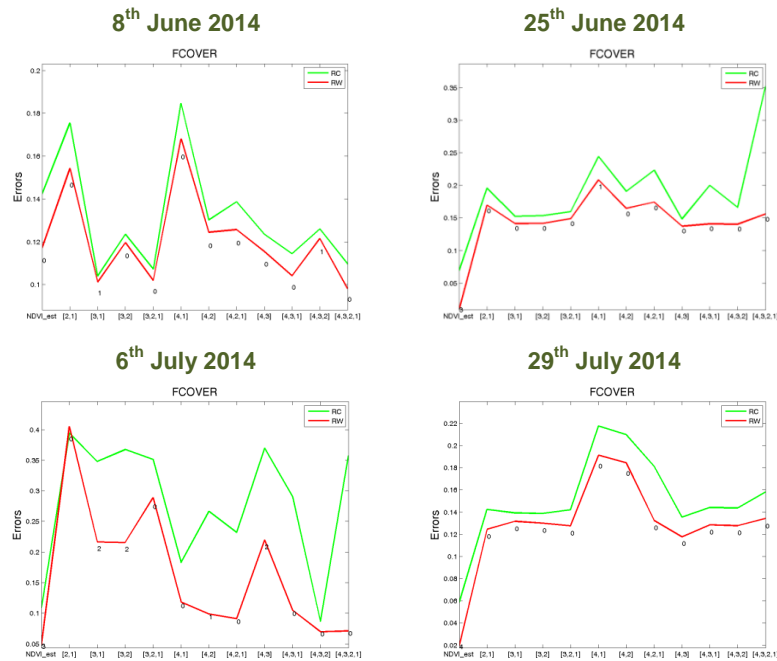


**Figure 19: Landsat-8 TOC Reflectance. Test of multiple regressions (TF) applied on different band combinations for FCover. Band combinations are given in abscissa (1=Green 2=Red, 3=NIR and 4=SWIR).**

### 6.2.3 The selected Transfer Function

The applied transfer function is detailed in

Table 8, along with its weighted (RW) and cross validated (RC) errors.

For the FCover, a simple linear relationship with NDVI was selected:

$$FCover = a + b \cdot NDVI \quad \text{Eq. (9)}$$

For the LAI<sub>eff</sub>, an exponential relationship with NDVI was selected according to Baret et al., (1989):

$$LAI_{eff} = a + b \cdot \ln \left( \frac{NDVI_{\infty} - NDVI}{NDVI_{\infty} - NDVI_s} \right) \quad \text{Eq. (10)}$$

Where  $b$  represents the extinction coefficient which depends on the average leaf angle inclination, solar zenith angle, diffuse reflectance and transmittance of the leaves. “ $b$ ” was set empirically with the ground data for each transfer function, as well as the residuals “ $a$ ”.  $NDVI_s$  represents the typical NDVI of bare soil areas and  $NDVI_{\infty}$  represents the NDVI of fully developed canopies, both assumed to be constant over the image.  $NDVI_s$  was set to 0.15 and  $NDVI_{\infty}$  to 0.95.

Note that few (4) additional estimated points based on the NDVI have been included for better constrain the transfer function (reported in Table 8) for very low values (between 0 and

0.2 FCover) due to the lack of observations for campaigns 2 and 3 (see Figure 15) and for very high values (FCover >0.85) in the first campaign. The additional LAI values were estimated from the NDVI image, based on the relationship proposed by Baret et al. (1989):

$$\widetilde{LAI} = -\frac{1}{k} \cdot \ln \left( \frac{NDVI_{\infty} - NDVI}{NDVI_{\infty} - NDVI_s} \right) \quad \text{Eq. (11)}$$

Where k is the extinction coefficient which depends on the average leaf angle inclination, solar zenith angle and diffuse reflectance and transmittance of the leaves. K was set to 0.6. NDVI is the vegetation index value of an individual pixel, NDVI<sub>s</sub> represents the typical NDVI of bare soil areas and NDVI<sub>∞</sub> were assumed to be constant over the image.

Whereas for the FCover, the additional points were estimated from Gutman and Ignatov (1998) as follows:

$$FCOVER = \left[ \frac{NDVI - NDVI_s}{NDVI_{\infty} - NDVI_s} \right] \quad \text{Eq. (12)}$$

with the same values than estimated LAI for NDVI<sub>s</sub> =0.15 and NDVI<sub>∞</sub>=0.95.

**Table 8: Transfer function applied to the whole site over Landsat-8 image for LAI<sub>eff</sub> and FCOVER. RW (weighted RMSE), RC (cross-validation RMSE).**

Variable	Band Combination	RW	RC
<b>8<sup>th</sup> June</b>		<b>First Campaign</b>	
<b>LAI<sub>eff</sub></b>	$0.001 - 1.667 \cdot \ln \left( \frac{NDVI_{\infty} - NDVI}{NDVI_{\infty} - NDVI_s} \right)$	0.089	0.419
<b>FCover</b>	$-0.169 + 1.344 \cdot NDVI$	0.117	0.011
<b>25<sup>th</sup> June</b>		<b>Second Campaign</b>	
<b>LAI<sub>eff</sub></b>	$0.033 - 1.368 \cdot \ln \left( \frac{NDVI_{\infty} - NDVI}{NDVI_{\infty} - NDVI_s} \right)$	0.070	0.400
<b>FCover</b>	$-0.181 + 1.225 \cdot NDVI$	0.010	0.070
<b>6<sup>th</sup> July</b>		<b>Third Campaign</b>	
<b>LAI<sub>eff</sub></b>	$0.222 - 1.537 \cdot \ln \left( \frac{NDVI_{\infty} - NDVI}{NDVI_{\infty} - NDVI_s} \right)$	0.500	0.650
<b>FCover</b>	$-0.176 + 1.228 \cdot NDVI$	0.050	0.100
<b>29<sup>th</sup> July</b>		<b>Fourth Campaign</b>	
<b>LAI<sub>eff</sub></b>	$-0.042 - 1.450 \cdot \ln \left( \frac{NDVI_{\infty} - NDVI}{NDVI_{\infty} - NDVI_s} \right)$	0.210	0.510
<b>FCover</b>	$-0.179 + 1.210 \cdot NDVI$	0.020	0.060

Figure 20 and Figure 21 show scatter-plots between ground measurements and their corresponding transfer function (TF) estimates. A good correlation is observed with points distributed mostly along the 1:1 line and no bias.

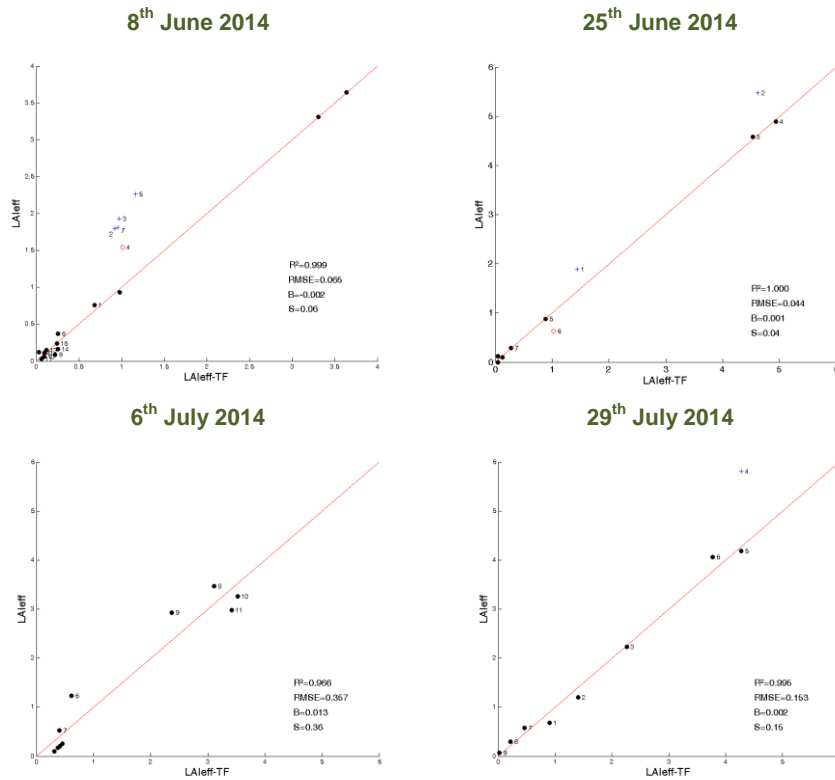


Figure 20: LAIeff, results for regression on NDVI over Landsat-8 image. Full dots: Weight>0.7. Empty dots: 0<Weight<0.7. Crosses: Weight=0.

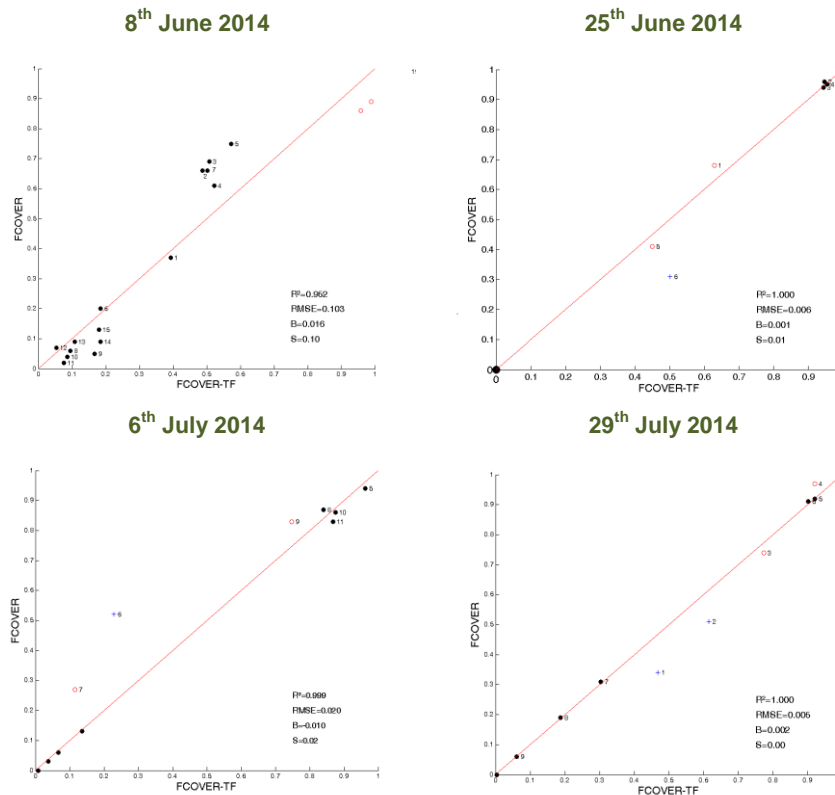
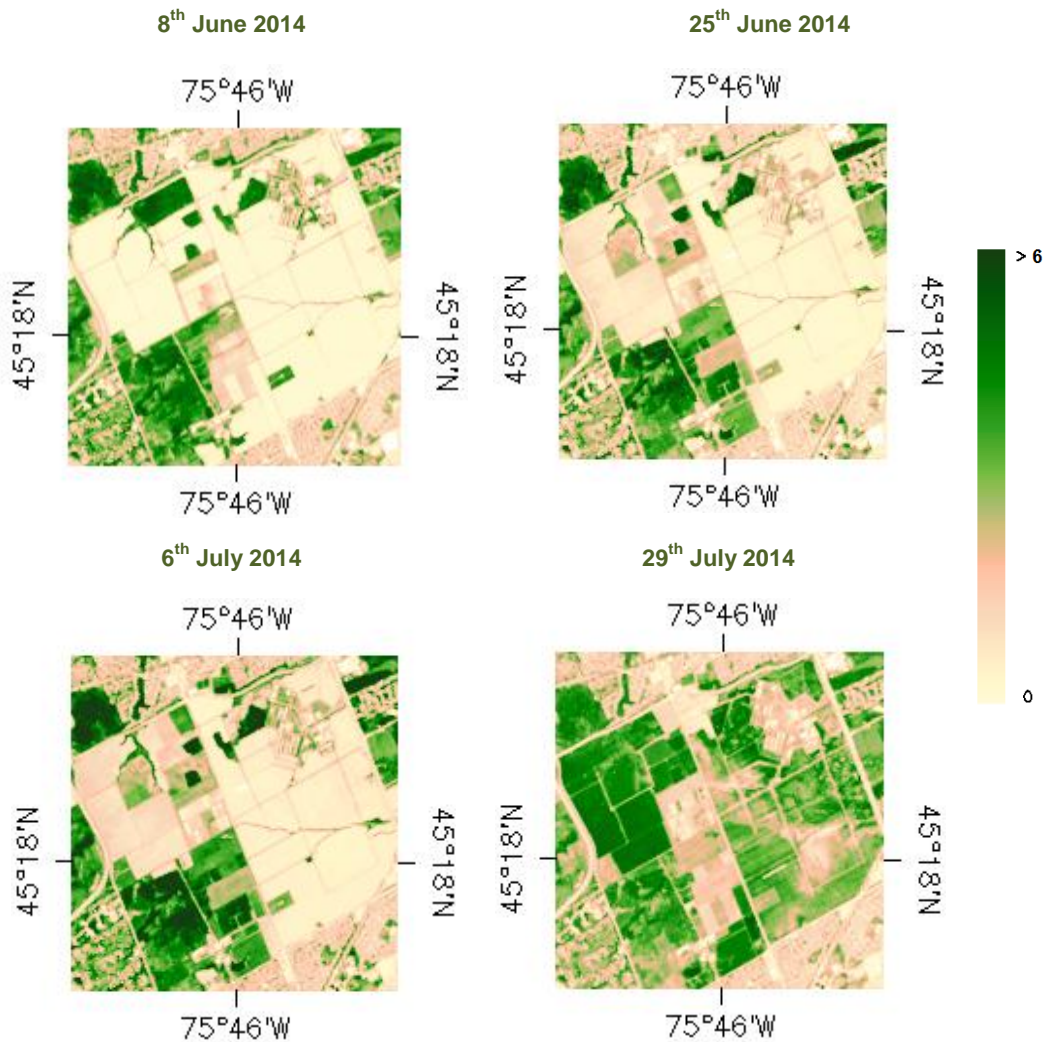


Figure 21: FCOVER results for regression on NDVI over Landsat-8 image. Full dots: Weight>0.7. Empty dots: 0<Weight<0.7. Crosses: Weight=0.



### 6.3. THE HIGH RESOLUTION GROUND BASED MAPS

The 5x5 km<sup>2</sup> high resolution maps are obtained applying the selected transfer function (Table 7) to the Landsat-8 TOC reflectance. Figure 22 and Figure 23 show the ground based maps provided for validation of satellite products. Figure 17 shows the Quality Flags included in the final product.



**Figure 22: Landsat-8 LAeff ground-based maps (5x5 km<sup>2</sup>) over the Ottawa site (Canada). The central date of each ground campaign is considered as representative of the ground map: 8<sup>th</sup> June (top left), 25<sup>th</sup> June (top right), 6<sup>th</sup> July (bottom left) and 29<sup>th</sup> July (bottom right), 2014.**



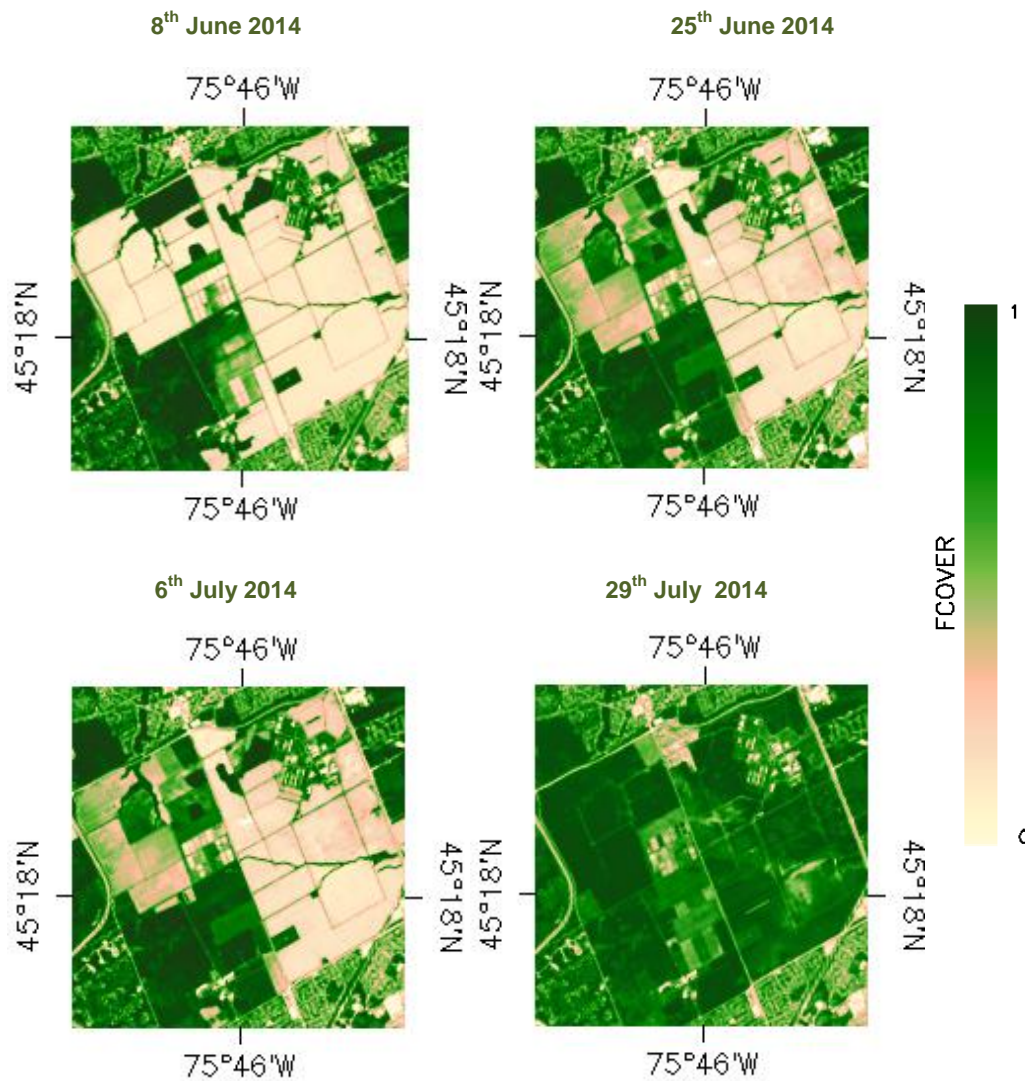


**Figure 23: Landsat-8 FCOVER ground-based maps (5x5 km<sup>2</sup>) over the Ottawa site (Canada). The central date of each ground campaign is considered as representative of the ground map: 8<sup>th</sup> June (top left), 25<sup>th</sup> June (top right), 6<sup>th</sup> July (bottom left) and 29<sup>th</sup> July (bottom right), 2014.**

Figure 24 shows, for the retrieved empirical maps, the typical exponential trend between LA<sub>eff</sub> and FCOVER for the four campaigns. Therefore, a good consistency between variables is achieved for the four dates. The quality flag map has not been taken into account for this evaluation.

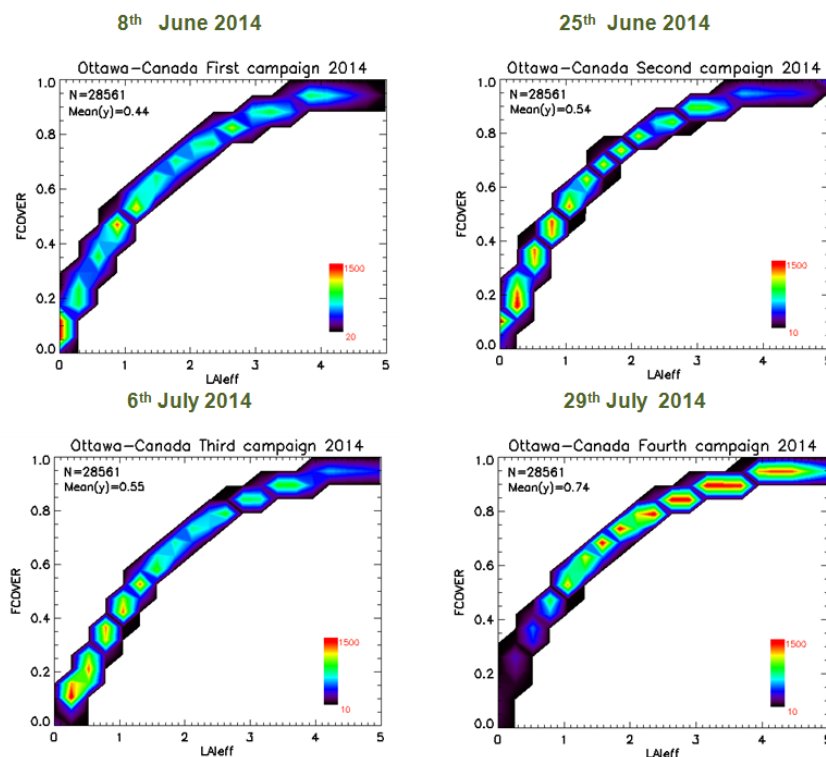


Figure 24: LA<sub>eff</sub> versus FCOVER scatter plots for the Landsat-8 ground-based maps. Ottawa site (Canada). 8<sup>th</sup> June (top left), 25<sup>th</sup> June (top right), 6<sup>th</sup> July (bottom left) and 29<sup>th</sup> July (bottom right)

### 6.3.1 Mean Values

Mean values of a 3x3 km<sup>2</sup> area centred in the test site are provided for validation of 1 km satellite products to reduce co-registration and PSF errors, and in agreement with the CEOS OLIVE direct dataset (Table 9). For the validation of coarser resolutions product (e.g. MSG products) a larger area should be considered. For this reason, empirical maps are provided at 5x5 km<sup>2</sup>.

Table 9. Mean values and standard deviation (STD) of the HR biophysical Landsat-8 maps for the selected 3 x 3 km<sup>2</sup> area at Ottawa site (Canada).

Ottawa Landsat-8 MEAN 3x3 km	LATITUDE		LONGITUDE	
	45.3056		-75.7673	
	Mean Values		STDV Values	
	LA <sub>eff</sub>	FCOVER	LA <sub>eff</sub>	FCOVER
8 <sup>th</sup> June	1.03	0.39	1.29	0.34
25 <sup>th</sup> June	1.46	0.48	1.49	0.30
6 <sup>th</sup> July	1.82	0.49	1.67	0.30
29 <sup>th</sup> July	2.79	0.79	1.15	0.15

Table 10 describes the content of the geo-biophysical maps in the nomenclature: "BIO\_YYYYMMDD\_SENSOR\_Site ETF\_Area" files, where:

BIO stands for Biophysical (LAI<sub>eff</sub> and FCOVER)

SENSOR = LANDSAT-8

YYYYMMDD = Campaign date

Site = Ottawa

ETF stands for Empirical Transfer Function

Area = 5x5 km<sup>2</sup>

**Table 10: Content of the dataset.**

Parameter	Dataset name	Range	Variable Type	Scale Factor	No Value
LAI effective	LAI <sub>eff</sub>	[0, 7]	Integer	1000	-1
Fraction of Vegetation Cover	FCover	[0, 1]	Integer	10000	-1
Quality Flag	QFlag	0,1,2 (*)	Integer	N/A	-1

(\*) 0 means extrapolated value (low confidence), 1 strict interpolator (best confidence), 2 large interpolator (medium confidence)

## 7. CONCLUSIONS

The FP7 ImagineS project continues the innovation and development activities to support the operations of the Copernicus Global Land service. One of the ImagineS demonstration sites is the Ottawa site in Canada.

This report first presents the ground data collected during a multi-temporal field campaign from May to August, 2014. The dataset includes a maximum of 15 elementary sampling units where standard digital photographs were taken and processed with the GreenCropTracker software to provide LA<sub>eff</sub> and F<sub>Cover</sub> values to characterize the main crops in the study area. Destructive green LAI and green PAI measured with the LI3100 Area Meter and FAPAR measurements obtained from the PAR balance with LI190SB and Li191 Quantum Sensor, have been also provided but only in a few points.

Ground-based maps have been derived using high resolution imagery (Landsat-8 TOC reflectance) according with the CEOS LPV recommendations for validation of low resolution satellite sensors. Transfer functions have been derived by multiple robust regressions between ESUs reflectance and the several biophysical variables. The transfer functions were based on Red and NIR (NDVI) due to the better consistency achieved over the whole image. A linear function with the NDVI was selected for F<sub>Cover</sub>, whereas a logarithmic function with the NDVI was selected for LAI. In the second and third campaign, three additional points based on semi-empirical NDVI functions were used to better constrain the transfer function for very low values due to the lack of observations for bare soils or sparse vegetation in those campaigns.

The RMSE values for the four transfer functions were very low 0.06, 0.04, 0.36 and 0.15 for LA<sub>eff</sub>; and 0.103, 0.006, 0.020 and 0.005 for F<sub>Cover</sub>, which shows the good fit of the ground measurements to the NDVI function.

The quality flag maps based on the convex-hull analysis show a good quality around the area that includes the ESUs. The percentages for the Landsat-8 transfer function of good interpolation capabilities for the 5x5 km<sup>2</sup> study area are 19%, 23%, 52% and 29%, which is quite low for three field campaigns due to the variability of the area and the low number of ESUs characterized.

The biophysical variable maps are available for the 5x5 km<sup>2</sup> area in geographic (18 North UTM projection WGS-84) coordinates at 30 m resolution. Mean values and standard deviation over a validation area of 3x3 km<sup>2</sup> for LA<sub>eff</sub> and F<sub>Cover</sub> were computed centered at the validation test site.

## 8. ACKNOWLEDGEMENTS

This study is supported by the FP7 IMAGINES project under Grant Agreement N°311766. Landsat 8-HR imagery is provided through the USGS Global Visualization service.

Thanks to the Agri-Food of Canada for providing the ground dataset.

## 9. REFERENCES

Baret, F., de Solan, B., Lopez-Lozano, R., Ma, K. and Weiss, M. (2010) GAI estimates of row crops from downward looking digital photos taken perpendicular to rows at 57.5° zenith angle: theoretical considerations based on 3D architecture models and application to wheat crops. *Agricultural and Forest Meteorology*. 150, 1393-1401.

Baret, F. and Fernandes, R. (2012). Validation Concept. VALSE2-PR-014-INRA, 42 pp.

Baret, F., G. Guyot and Major, D. (1989). Crop biomass evaluation using radiometric measurements. *Photogrammetria* 43:241-256.

Camacho, F., Cernicharo, J., Lacaze, R., Baret, F., and Weiss, M. (2013). GEOV1: LAI, FAPAR Essential Climate Variables and FCOVER global time series capitalizing over existing products. Part 2: Validation and intercomparison with reference products. *Remote Sensing of Environment*, 137: 310-329.

Demarez, V., Duthoit, S., Baret, F., Weiss, M. and Dedieu, G. (2008). Estimation of leaf area and clumping indexes of crops with hemispherical photographs. *Agricultural and Forest Meteorology*. 148, 644-655.

Fernandes, R., Plummer, S., Nightingale, J., et al. (2014). Global Leaf Area Index Product Validation Good Practices. CEOS Working Group on Calibration and Validation - Land Product Validation Sub-Group. *Version 2.0.1: Public version made available on LPV website*.

Gutman, G. and Ignatov, A. (1998). The derivation of green vegetation fraction from NOAA/AVHRR data for use in numerical weather prediction models. *Int. J. Remote Sensing*, 19. 1533-1543.

Goudriaan, J. (1988). The bare bones of leaf-angle distribution in radiation models for canopy photosynthesis and energy exchange. *Agricultural and Forest Meteorology*. 43, 155-169.

JECAM, (2014). GEO Joint Experiment for Crop Assessment and Monitoring (JECAM): 2014 Progress Report. (available on-line at <http://www.jecam.org/?/charter/annual-reports>)

Lang, A.R.G., and Xiang, Y. (1986). Estimation of leaf area index from transmission of direct sunlight in discontinuous canopies. *Agricultural and Forest Meteorology* 37, 229-243.

LI-COR Inc., Lincoln, Nebraska, (2013). [http://envsupport.licor.com/docs/LI-3100-Instruction\\_Manual.pdf](http://envsupport.licor.com/docs/LI-3100-Instruction_Manual.pdf), [http://envsupport.licor.com/docs/LI-190SB\\_Instruction\\_Manual.pdf](http://envsupport.licor.com/docs/LI-190SB_Instruction_Manual.pdf), [http://envsupport.licor.com/docs/LI-191R\\_Instruction\\_Manual.pdf](http://envsupport.licor.com/docs/LI-191R_Instruction_Manual.pdf)

LI-COR Inc., Lincoln, Nebraska, (1992). [http://envsupport.licor.com/docs/LAI-2200\\_Instruction\\_Manual.pdf](http://envsupport.licor.com/docs/LAI-2200_Instruction_Manual.pdf)

Liu, J., and Pattey, E. (2010). Retrieval of leaf area index from top-of-canopy digital photography over agricultural crops. *Agricultural and Forest Meteorology* 150 (2010) 1485-1490

Liu, J., Pattey, E. and Jégo, G. (2012). Assessment of vegetation indices for regional crop green LAI estimation from Landsat images over multiple growing seasons. *Remote sensing Environment*, 123,347-358

Liu, J., Pattey, E. and Admiral, E. (2013). Assessment of in situ crop LAI measurement using unidirectional view digital photography. *Agricultural and Forest Meteorology* 169 (2013) 25-34

Martínez, B., García-Haro, F. J., and Camacho, F. (2009). Derivation of high-resolution leaf area index maps in support of validation activities: Application to the cropland Barrax site. *Agricultural and Forest Meteorology*, 149, 130–145.

Morisette, J. T., Baret, F., Privette, J. L., Myneni, R. B., Nickeson, J. E., Garrigues, S., et al. (2006). Validation of global moderate-resolution LAI products: A framework proposed within the CEOS land product validation subgroup. *IEEE Transactions on Geoscience and Remote Sensing*, 44, 1804–1817.

Nilson, T., (1971). A theoretical analysis of the frequency of gaps in plant stands. *Agric. Forest Meteorol.* 8, 25–38.

Warren Wilson, J. (1960). Inclined point quadrats. *New Phytol.*, 59 (1960), pp. 1–7

Welles, J.M. and Norman, J.M., (1991). Instrument for indirect measurement of canopy architecture. *Agronomy J.*, 83(5): 818-825.